Revision 2

# P-V-T measurements of $Fe_3C$ to 117 GPa and 2100 K: implications for stability of $Fe_3C$ phase at core conditions

Chris McGuire[1], Tetsuya Komabayashi[1], Samuel Thompson[1] and Geoffrey Bromiley[1], Takayuki Ishii[2], Eran Greenberg[3*], Vitali B. Prakapenka[3]

[1]School of GeoSciences and Centre for Science at Extreme Conditions, University of Edinburgh EH9 3FE, UK

[2] Bayerisches Geoinstitut, University of Bayreuth, 95440 Bayreuth, Germany

[3] Center for Advanced Radiation Sources, The University of Chicago, Chicago, IL, 60637, USA

Corresponding author:

Chris McGuire

e-mail: C.McGuire@ed.ac.uk

[*] Present address: Applied Physics Department, Soreq Nuclear Research Center (NRC), Yavne 81800, Israel

Abstract

We report the thermal equation of state of the nonmagnetic $Fe_3C$ phase based on in-situ X-ray diffraction (XRD) experiments to 117 GPa and 2100 K. High-pressure and temperature unit-cell volume measurements of $Fe_3C$ were conducted in a laser-heated diamond anvil cell. Our pressure-volume-temperature (P-V-T) data together with existing data were fit to the Vinet equation of state with the Mie-Grüneisen-Debye thermal pressure model, yielding $V_0$ = 151.6(12) $Å^3$, $K_0$ = 232(24) GPa, $K_0'$ = 5.09(46), $\gamma_0$= 2.3(3), and q = 3.4 (9) with $\theta_0$ = 407 K (fixed). The high-T data were also fit to the thermal pressure model with a constant $\alpha K_T$ term, $P_{th} = \alpha K_T(\Delta T)$, and there is no observable pressure or temperature dependence, which implies minor contributions from the anharmonic and electronic terms. Using the established EoS for $Fe_3C$, we made thermodynamic calculations on the P-T locations of the breakdown reaction of $Fe_3C$ into $Fe_7C_3$ and Fe. The reaction is located at 87 GPa and 300 K and 251 GPa and 3000 K. An invariant point occurs where Fe, $Fe_3C$, $Fe_7C_3$, and liquid are stable, which places constraints on the liquidus temperature of the outer core, namely inner core crystallization temperature, as the inner core would be comprised by the liquidus phase. Two possible P-T locations for the invariant point were predicted from existing experimental data and the reaction calculated in this study. The two models result in different liquidus phase relations at the outer core-inner core boundary pressure: $Fe_3C$ at 5300 K and $Fe_7C_3$ at 3700 K. The $Fe_7C_3$ inner core can account for the density, as observed by seismology, while the $Fe_3C$ inner core cannot. The relevance of the system Fe-C to Earth's core can be resolved by constructing a thermodynamic model for melting relations under core conditions as the two models predict very different liquidus temperatures.

## INTRODUCTION

Earth's liquid outer core and solid inner core are known to be less dense than pure iron by 7 - 10 and 3 - 5%, respectively (Dewaele et al. 2006; Komabayashi 2014; Fei et al. 2016; Kuwayama, et al. 2020). Carbon is a possible candidate as a light-alloying element in the Earth's core, along with S, Si, O and H (Hirose et al. 2013). Cosmochemical evidence suggests that carbon was abundant in the solar nebula during planetary accretion and it is present in CI chondrites at 3.4 wt% (Wood 1993; McCammon 2020). The fate of carbon during Earth's accretion and core formation is open to debate. Earth's mantle is depleted in carbon compared with chondrites (McDonough and Sun 1995; Palme and O'neill 2003), leading to the possible conclusion that carbon was either lost from Earth by volatilization during impacts or that carbon was incorporated into a magma ocean during accretion, but lost from the mantle by sequestration into the core. At high pressures corresponding to Earth's upper mantle, carbon volatility decreases, lending support to the hypothesis that carbon should be incorporated into a magma ocean in terrestrial planets (Wood 1993). Metal/silicate partitioning experiments at pressures corresponding to a shallow magma ocean support the assertion that carbon is likely to partition into the metal phase during core-formation (Nakajima et al. 2009; Siebert et al. 2011; Dasgupta et al. 2013). At higher pressures corresponding to a deep magma ocean, delivery of carbon to the core may be enhanced by clustering of carbon around iron atoms in silicate melt (Solomatova et al. 2019). These lines of reasoning lead us to consider the possibility that carbon is present in Earth's core as a significant (> 1.5 wt%) light element.

Phase relations in the system Fe-C under high pressure and temperature have been examined by experiment and first-principles calculations. Wood (1993) suggested that $Fe_3C$ may compose the inner core from thermodynamic calculations to 330 GPa based on his own melting experimental data to 5 GPa. Experiments at higher pressures up to 29 GPa showed instead that $Fe_7C_3$ would be the first phase to crystallize out of a carbon-rich liquid core

(Nakajima et al. 2009). $Fe_3C$ and $Fe_7C_3$ phases have different carbon contents, thermoelasticity and physical properties and therefore their stability relations are critically important for models of a carbon-bearing inner core. Both of these iron carbides have been shown to plausibly match some solid-state physical properties of the inner core, such as shear wave velocity and Poisson's ratio (Gao et al. 2008; 2011; Chen et al. 2014; Prescher et al. 2015; Chen et al. 2018).

A key reaction for the stability relation between $Fe_3C$ and $Fe_7C_3$ is,

$$3Fe_3C = Fe_7C_3 + 2Fe \quad (1)$$

which is an equilibrium univariant reaction. This was first inferred by Lord et al. (2009) from the topology of high-pressure melting curves of $Fe_3C$ and $Fe_7C_3$. Reaction (1) was later examined experimentally in a laser-heated diamond anvil cell (DAC) with in-situ X-ray diffraction (XRD) by Liu et al. (2016), who placed its boundary at about 150 GPa. This observation is contradicted, however, by Tateno et al. (2010)'s in-situ XRD measurements of the formation of $Fe_3C$ phase in their Fe sample in the DAC upon laser heating at about 340 GPa. More recent in-situ XRD experiments also observed $Fe_3C$ to pressures greater than 250 GPa (Takahashi et al. 2020). Mookherjee et al. (2011b) found that $Fe_3C$ is energetically stable at all pressures to the center of the Earth from first-principles calculations on the energetics of reaction (1) at T = 0. On the other hand, Mashino et al. (2019) reported the $Fe_3C$ phase as a liquidus phase in their melting experiments in the system Fe-C to 203 GPa, but placed the possible occurrence of reaction (1) at 255 GPa from chemical and textural analyses of recovered samples. As such, the high-pressure stability of $Fe_3C$ has not been agreed upon.

Another important reaction for $Fe_3C$ is melting. Tateno et al. (2010) showed solid $Fe_3C$ would be stable to 5520 K at about 340 GPa, which may be consistent with recent in-situ XRD measurements of the melting curve of $Fe_3C$ by Takahashi et al. (2020) to 4310 K at 192 GPa. In contrast, Mashino et al. (2019) reported the eutectic temperature of 3570 K at 255 GPa. As predicted by Lord et al. (2009), the melting reaction $Fe_3C$=$Fe_7C_3$+liquid and

eutectic reaction Fe+$Fe_3C$=liquid should intersect at a high pressure, and therefore the two reactions should occur at similar temperatures under core pressures. This implies that the eutectic temperature constrained by Mashino et al. (2019) can be a proxy of the melting temperature of $Fe_3C$ via the reaction $Fe_3C$=$Fe_7C_3$+liquid. As such, there is likely a significant discrepancy in the high-temperature stability of $Fe_3C$ in the DAC experiments between Tateno et al. (2010) and Takahashi et al. (2020), and Mashino et al. (2019). Indeed, we will show from analysis of the reaction topology of melting relations that these experimental results are inconsistent with each other.

On the determination of the P-T locations of reaction (1), it may be difficult to examine the reaction by in-situ XRD experiment. If the $Fe_7C_3$ phase is present as the orthorhombic structure (Prescher et al., 2015; Lai et al., 2018) rather than a hexagonal structure (Nakajima et al. 2011), its diffraction peaks would be aliased with hcp Fe and $Fe_3C$, depending on the pressure (Aprilis et al. 2019). Mashino et al. (2019)'s experiments were quench experiments from melting and interpretation of a quenched texture may be ambiguous. Both XRD and textural analyses will be more complicated if $Fe_7C_3$ were synthesized by reaction of iron-alloy sample with the diamonds during laser heating, rather than as a result of reaction (1) (Aprilis et al. 2019). An alternative promising approach to the P-T locations of reaction (1) is thermodynamic phase equilibrium calculation (e.g., Wood 1993). A more recent database for the system Fe-C was established by Fei and Brosh (2014) but their database may not be applicable to reaction (1) since their focus was on reproducing the eutectic relations based on multianvil experimental data which is far lower in pressure than reaction (1) at 150-250 GPa. The thermodynamic database for pure Fe, which can be applicable up to the center of the Earth, was already available (Komabayashi 2014), whereas those for the carbides have yet to be refined due to the lack of precise equations of state (EoS) for the phases. The EoS for the carbides also has direct implications for their densities under inner core conditions.

The room temperature compressibility for $Fe_3C$ has been measured with powder and single crystal samples in the DAC up to 170 GPa and 60 GPa, respectively (Scott et al. 2001; Li et al. 2002; Ono and Mibe 2010; Sata et al. 2010; Prescher et al. 2012). However, the volume of $Fe_3C$ under simultaneous high pressure and temperature conditions has been measured up to 32 GPa in a multi-anvil experiment and inferred from a shock compression experiment (Litasov et al. 2013; Hu et al. 2019; Liu et al., 2020). In order to discuss the density of the core and the P-T location of reaction (1), a self-consistent thermal EoS for $Fe_3C$ should be established based on higher P-T experimental data. In the case of $Fe_7C_3$, Nakajima et al. (2011) constructed a consistent thermal EoS based on their own static experiments up to 71.5 GPa and simultaneous high-P-T experiments to 30 GPa and 1973 K.

Here, we conducted high-pressure and high-temperature unit-cell volume measurements on $Fe_3C$ by in-situ XRD to 117 GPa and 2100 K and constructed its thermal EoS. Using the constructed EoS of $Fe_3C$, we calculated the P-T locations of reaction (1) by thermodynamic calculation and discuss the stability of $Fe_3C$ under core conditions.

## EXPERIMENTAL PROCEDURE

The $Fe_3C$ starting material was synthesized from Fe and high purity graphite powder in an MgO capsule held at 2.0 GPa and 1473 K for 24 hours, in a piston cylinder apparatus at The University of Edinburgh. The molar ratio of Fe:C for the starting powders was 2.9701:1, slightly enriched in C, in order to ensure the run product was not in the Fe−$Fe_3C$ stability field upon minor volatilization of carbon (Zhang et al. 2018). The $Fe_3C$ sample was ground into a powder under acetone, and phase purity was confirmed by X-ray diffraction. The unit-cell volume of the synthesized sample is 155.09(5) $Å^3$.

Powder $Fe_3C$ samples were prepared as flakes, approximately 10 μm thick. The sample and KCl pressure transmitting medium were loaded in a gasketed DAC with beveled 150 μm

diameter culet diamonds. The gasket material was rhenium, pre-compressed to ~40 μm thick, and a 50 μm diameter hole drilled by a spark eroder (BETSA). The KCl was kept in an oven at 110 °C, before being compressed into pellets approximately 15 μm thick and loaded above and below the flake of $Fe_3C$. The cell was kept overnight in a vacuum oven at 110 °C before closing.

In-situ X-ray diffraction experiments were carried out at the Advanced Photon Source, GSECARS beamline 13 ID-D, at a wavelength of 0.3344 Å. Powder diffraction images were collected on a 2D Pilatus 1 M CdTe detector. $LaB_6$ was used to calibrate the beam-center, detector tilts and sample-to-detector distance. Calibration, image processing and data reduction were completed using the program DIOPTAS (Prescher and Prakapenka 2015). High temperatures were generated by double-sided heating with ytterbium fiber lasers operating at 1.064 μm wavelength (Prakapenka et al. 2008). Experimental temperatures were measured by spectroradiometry, using the greybody approximation. The alignment of the X-ray beam and the laser was checked between heating cycles by fluorescence of the KCl pressure transmitting medium. The laser heating spot is approximately 25 μm in diameter, and the X-ray beam is 3 x 3 $\mu m^2$ at FWHM (Prakapenka et al., 2008). The duration of heating was limited to 1 second, synchronized with high-temperature XRD pattern collection. The high temperature XRD pattern was followed immediately by collection of a quench XRD pattern. In Run 3 at each pressure, the sample was heated to approximately 1500 K to relieve the nonhydrostatic stress, and the room temperature volume was recorded upon quench.

## RESULTS

### In-situ XRD experiment

Three separate in-situ XRD runs were carried out. Runs 1 and 2 were 300 K compression, following quenching from double-sided laser heating and in-situ high

177 temperature measurements during laser heating. Run 3 was 300 K compression only, in which
178 quench diffraction patterns were collected following single-sided laser heating at each pressure
179 step. Selected room temperature diffraction patterns up to the maximum pressure of 117 GPa
180 are shown in Figure 1. The unit-cell volume of orthorhombic $Fe_3C$ at high pressures and
181 temperatures was determined from at least 10 diffraction peaks among the following: (020),
182 (111), (201), (211), (102), (220), (031), (112), (022), (221), (212), and (231). The standard
183 deviations of lattice parameters were calculated from least squares regression and the error on
184 each parameter was propagated to give the uncertainty in volume.

185 The experimental pressure was determined from the thermal equation of state of KCl at
186 both room temperature and elevated temperature (Tateno et al., 2019). The KCl pressure
187 transmitting medium experiences a range of temperatures in the axial direction from a
188 maximum of the spectroradiometric temperature at the KCl/$Fe_3C$ interface to approximately
189 room temperature at the KCl/diamond interface. Accordingly, we adopted the temperature
190 correction proposed by Campbell et al. (2009) which accounts for geometric averaging of the
191 intersection of the temperature gradient and the X-ray beam. The uncertainty in pressure is
192 determined by error propagation of measured volume of KCl and each of EoS parameters for
193 KCl given in Tateno et al. (2019).

194 Heating cycles were conducted in approximately 50 K steps from 1500 K to 2100 K; at
195 pressures below 50 GPa, we limited the temperature to 1800 K to avoid melting the sample. An
196 example of XRD data from a heating cycle at 99.5 GPa is shown in Figure 2, with the quench
197 pattern. During heating, a few minor peaks appeared and are also present in the quench pattern.
198 These peaks are present in all the heating runs and can be indexed with $Fe_7C_3$ (Nakajima et al.
199 2011). We interpret the formation of $Fe_7C_3$ as a result of reaction between the sample and
200 carbon contaminated from the diamond anvils or minor excess carbon in the starting material,
201 rather than a result of reaction (1), because we did not observe hcp Fe peaks (Fig. 2). Indexed

peaks used to calculate the volume for $Fe_3C$ and KCl are indicated in Figure 2 by red triangles and orange circles, respectively. The unit-cell volume versus pressure up to 117 GPa and temperature up to 2100 K is shown in Figure 3. Our room temperature measurements are also compared in Figure 3a with previous measurements. At room temperature, our data is indistinguishable from other powder diffraction data sets over the same pressure range (Li et al. 2002; Ono and Mibe 2010; Sata et al. 2010; Litasov et al. 2013). Our P-V-T measurements and their uncertainties are shown in Table 1.

**Equation of state**

The room temperature (300 K, $T_0$) unit-cell volume data were fit to the Vinet EoS (Vinet et al., 1987):

$$P(V,T_0) = 3K_0(1-x)x^{-2}exp\left[\frac{3}{2}(K_0'-1)(1-x)\right] \qquad (2)$$

where $x = \left(\frac{V}{V_0}\right)^{\frac{1}{3}}$, $V_0$ and $K_0$ are the volume and bulk modulus at 300 K and 1 bar, and $K_0'$ is the pressure derivative of the bulk modulus. As discussed below in detail, the $Fe_3C$ phase studied here is nonmagnetic, and we therefore only included Sata et al. (2010)'s data among the existing reports as their measurements were made at pressures greater than 50 GPa which is higher than the magnetic transition pressures (Lin et al. 2004; Prescher et al. 2012; Chen et al. 2018). Although Sata et al. (2010)'s data covers a wide pressure range to 187 GPa, we adopted their data to 100 GPa in order to avoid the possible phase transition to $Fe_7C_3$ and Fe (reaction 1) at greater pressures. We discuss this later in more detail. We recalculated the pressure values in Sata et al. (2010)'s P-V dataset based on the MgO pressure scale by Sokolova et al. (2013) who produced a set of consistent pressure scales. The pressure scale in this study is the EoS of KCl by Tateno et al. (2019) which was based on Sokolova et al. (2013)'s pressure scale. A least squares fit to the 300 K unit-cell volume data of $Fe_3C$ in this study and Sata et al. (2010)

This is the peer-reviewed, final accepted version for American Mineralogist, published by the Mineralogical Society of America.
The published version is subject to change. Cite as Authors (Year) Title. American Mineralogist, in press.
DOI: https://doi.org/10.2138/am-2021-7581. http://www.minsocam.org/

yielded $V_0$ = 155.0(37) Å$^3$, $K_0$ = 172 (54) GPa, and K' = 6.4 (12). As the non-magnetic state is non recoverable to 1 bar and the lowest pressure data was collected at 29 GPa, the resulting 1 bar parameters show large uncertainties.

A thermal EoS for the P-V-T dataset was then constructed using the thermal pressure formalism.

$$P(V,T) = P(V,T_0) + \Delta P_{Th} \quad (3)$$

where $P(V,T_0)$ is the pressure at $V$ and $T_0$, and $\Delta P_{Th}$ is the thermal pressure. The first term on the right hand side is obtained from the room temperature EoS. We fit two different thermal pressure terms (Jackson and Rigden 1996): (1) Mie-Grüneisen Debye (MGD) model, and (2) $\alpha K_T$ model.

(1) The thermal pressure can be evaluated from the internal thermal energy as given in the MGD model (Jackson and Rigden 1996):

$$\Delta P_{Th} = \frac{\gamma}{V}\left(E_{Th}(V,T) - E_{Th}(V,T_0)\right) \quad (4)$$

where γ is the vibrational Grüneisen parameter and $E_{Th}$ is the internal thermal energy:

$$E_{Th} = \frac{9nRT}{\left(\theta/T\right)^3}\int_0^{\theta/T}\frac{z^3}{(e^z-1)}dz \quad (5)$$

The Debye temperature is denoted as $\theta$; $n$ and R are the number of atoms per formula unit and the gas constant, respectively. The MGD model parameterizes the volume dependence of the Grüneisen parameter and Debye temperature as follows:

$$\gamma(V) = \gamma_0\left(\frac{V}{V_0}\right)^q \quad (6)$$

$$\theta = \theta_0 exp\left[\frac{(\gamma_0-\gamma(V))}{q}\right] \quad (7)$$

where $\theta_0$ and $\gamma_0$ are the ambient condition Debye temperature and vibrational Grüneisen parameter, respectively. The parameter q is a free parameter to express the volume dependence of the Grüneisen parameter.

We fixed the Debye temperature at 407 K (Litasov et al. 2013), since this parameter is not well constrained by fitting a P-V-T dataset in which temperatures far exceed the Debye temperature (Noguchi et al. 2013). Because there was no report on $\theta_0$ for the nonmagnetic $Fe_3C$ phase, we adopted the $\theta_0$ value of 407 K for the paramagnetic phase, which is a reasonable assumption as $\theta_0$ does not seem to significantly depend on the magnetic property of $Fe_3C$ (Litasov et al. 2013). The room-T data were included as well as the high-T data in the dataset for the fit. A simultaneous fit to the remaining five parameters of MGD EoS yielded: $V_0$ = 151.6(12) Å$^3$, $K_0$ = 232(24) GPa, $K_0'$ = 5.09(46), $\gamma_0$= 2.3(3), and q = 3.4(9). The resulting $V_0$ shows a smaller value than measured at 1 bar (V = 155.09(5) Å$^3$) for the ferromagnetic phase. As the nonmagnetic phase is a high-pressure phase, the result of the fit is reasonable. The fit along several isotherms is shown in Figure 3.

(2) Another thermal pressure model is the $\alpha K_T$ model:

$$\Delta P_{Th} = \alpha K_T * (T - T_0) \quad (8)$$

where $\alpha$ is the thermal expansion coefficient, $K_T$ is the isothermal bulk modulus and $T_0$ is the reference temperature (300 K). A least squares fit to our high-$T$ data yielded $\alpha K_T$ of 0.0068 ± 0.0002 GPa/K. From $K_0$ of 232 GPa, this gives $\alpha_0$ = 2.9(3)*10$^{-5}$/K where $\alpha_0$ is the thermal expansivity at 1 bar and 300 K, which is close to the 1 bar measurement, 4.1*10$^{-5}$, for the paramagnetic phase (Wood et al. 2004). This confirms $\alpha K_T \sim \alpha_0 K_0$, which justifies our Debye temperature of 407 K, close to 300 K. We show the misfit between the observed pressure and the calculated pressure from the MGD model and $\alpha K_T$ model in Figure 4.

**Thermodynamic calculation on $3Fe_3C = Fe_7C_3 + 2Fe$**

The high-pressure phase stability of $Fe_3C$, defined by reaction (1), was calculated from the Gibbs free energy, which is expressed as the sum of an ambient pressure term and an integral over the volume.

$$G(P,T) = G(P_0,T) + \int_{P_0}^{P} V(P,T)\, dP \quad (9)$$

The first term in the right hand side of equation 9, $G(P_0,T)$, is given by the ambient pressure thermochemistry of the relevant phases. For the non-magnetic carbide phases, $Fe_3C$ and $Fe_7C_3$, $G(P_0,T)$, is formulated from Hallstead et al. (2010) and Fei and Brosh (2014), respectively (Table 3). For hcp Fe, we use the analysis from Komabayashi (2014) (Table 3). The second term in equation 9 is obtained by integrating the volume with respect to pressure. The thermal EoS adopted in the calculations are hcp Fe (Dewaele et al. 2006) which was included in the Fe database in Komabayashi (2014), $Fe_3C$ (this study), and $Fe_7C_3$ (Nakajima et al. 2011). In order to draw precise conclusions, the pressure scale used in the EoS for each phase should be consistent. The EoS for hcp Fe by Dewaele et al. (2006) and for $Fe_3C$ in this study are consistent with a set of pressure scales proposed by Sokolova et al. (2013). We recalculated the experimental pressure values in Nakajima et al. (2011) against the MgO scale by Sokolova et al. (2013) and fit the data to the Vinet-MGD EoS. Nakajima et al. (2011) fit all the MGD parameters including the Debye temperature and obtained $\theta_0$ = 920 K. We fixed $\theta_0$ for $Fe_7C_3$ at 665 K so that it reproduces the thermal expansivity at 1 bar 300 K by Litasov et al. (2015). These MGD parameters were re-fit to the Anderson-Grüneisen (AG) model for integration purposes for equation 9 (Wood 1993; Komabayashi 2014). The AG model treats the pressure effect on the thermal expansivity using the Anderson-Grüneisen parameter, $\delta_T$ (Anderson et al. 1992):

$$\frac{\partial ln\alpha}{\partial lnV} = \delta_T = \delta_0 \eta^{\kappa} \quad (10)$$

where $\eta \equiv V/V_0$, $\delta_0$ is the value of $\delta_T$ at 1 bar and $\kappa$ is a dimensionless parameter. This equation yields:

$$\frac{\alpha}{\alpha_0} = exp\left[-\frac{\delta_0}{\kappa}(1-\eta^{\kappa})\right] \quad (11)$$

where $\alpha_0$ is the thermal expansivity at 1 bar. Note that the $\alpha_0$ value is assumed to be constant and independent of temperature in this study. The parameters of the AG model are listed in Table 2.

The phase boundary is calculated by finding where the Gibbs free energy of reaction (1), 3 $Fe_3C$ = $Fe_7C_3$ + 2 Fe, is equal to zero. The calculation yields equilibrium transition pressures for the breakdown reaction that are 87 GPa at 300 K, 140 GPa at 1000 K, and 251 GPa at 3000 K (Fig. 5). The P-T locations of the boundary are compared with earlier reports in Figure 6 (Tateno et al. 2010; Liu et al. 2016; Mashino et al. 2019; Takahashi et al. 2020). Among them, data in Tateno et al. (2010) and Mashino et al. (2019) are consistent with our calculated boundary for reaction 1.

## DISCUSSION

### Thermal EoS of $Fe_3C$

Solid $Fe_3C$ is known to go through a series of second-order magnetic transitions as the temperature or pressure changes, which could affect its elastic properties. At 1 bar and room temperature, $Fe_3C$ is ferromagnetic (FM), and undergoes a high-temperature transition to paramagnetic (PM) state with a Curie temperature, $T_C$ = 460 K (Wood et al. 2004; Walker et al. 2015). At elevated pressure, experiments have shown that $T_C$ reduces to room temperature, although there are a range of pressures reported from 4.3-6.5 GPa (Gao et al. 2008;Walker et al. 2015) to 8-10 GPa (Duman et al. 2005; Prescher et al. 2012). At higher pressure, another second-order transition to the non-magnetic (NM) phase is expected to occur. An X-ray emission spectroscopy study showed the loss of Fe-$K_\beta$ satellite peak occurred at 25 GPa (Lin et al. 2004). A similar transition pressure of 22 GPa was later reported from single crystal Mössbauer spectroscopy measurements (Prescher et al. 2012). Recently, Chen et al. (2018) suggested that the transition to the NM phase would take place over a wide pressure range of

323 10-50 GPa based on their X-ray emission spectroscopy measurements. Ono and Mibe (2010)
324 discussed that the transition pressure to the NM phase would be placed at 55 GPa from an
325 abrupt reduction in volume during compression by powder XRD measurements at 300 K.
326 From theoretical calculations at T = 0, magnetic collapse was predicted to occur at 55 GPa
327 (Ono and Mibe 2010) or above 60 GPa (Vocadlo et al. 2002; Mookherjee 2011a). It should be
328 noted that the theoretical studies predict the FM/NM transition, rather than the two magnetic
329 transitions that are observed experimentally (Walker et al. 2015). As such, the experimentally
330 constrained transition pressures seem to be lower than the theoretical values.
331 Our P-T data coverage for the EoS fit is 29-117 GPa and 300-2100 K which is in the
332 stability field of the NM phase based on experimental studies (Lin et al. 2004; Prescher et al.
333 2012). In addition, according to Chen et al. (2018), 29 GPa corresponds to about 80%
334 completion of the transition to the NM phase. Since the magnetic transition is second order, it
335 would not be detected by our XRD data (Prescher et al. 2012) even if the transition occurred at
336 the much higher pressure of 60 GPa (Vocadlo et al. 2002). Indeed we fit the volume data to a
337 single thermal EoS and the misfits show no pressure or temperature dependence (Fig. 4).
338 Therefore, our single EoS can reasonably describe the compression behavior of nonmagnetic
339 $Fe_3C$. In addition, the fitted $V_0$ in this study is significantly smaller than that for FM/PM $Fe_3C$
340 (Scott et al. 2001; Li et al. 2002; Litasov et al. 2013) (Table 2). This is likely because we fit
341 PVT data over the pressure range of the nonmagnetic phase, which becomes less compressible
342 than the paramagnetic phase. Ono and Mibe (2010) associated the abnormal reduction in
343 volume at 55-60 GPa observed in their experiments with the magnetic transition from
344 ferromagnetic to nonmagnetic derived from their own first-principles calculations. We did not
345 observe any indication of the magnetic transition in our unit-cell volume data or in the lattice
346 parameters at those pressure ranges. As Ono and Mibe (2010)'s experiment measured volumes
347 only in a compression run, a future experimental investigation should make both compression

348 (normal) and decompression (reversal) runs as was made on ferropericlase (Fei et al. 2007;
349 Komabayashi et al. 2010).

350 We adopted the data of Sata et al. (2010) up to 101 GPa in the fit together with our own
351 data set, although they collected data up to 187 GPa. Sata et al. (2010) employed thermal
352 annealing before collecting the unit-cell volume at 300 K and therefore the quench pattern
353 might be contaminated by the high-pressure phases, $Fe_7C_3$ and Fe if reaction (1) took place
354 during annealing. Note that the transition pressure from our thermodynamic calculations at 300
355 K is 87 GPa. In fact, Sata et al. (2010) observed $Fe_7C_3$ in their quenched XRD patterns at 187
356 GPa. The other product, Fe might have been oxidized in the DAC sample chamber and
357 reacted with the pressure marker MgO used in their experiments to form (Mg,Fe)O. The
358 unit-cell volume of ferropericlase is larger than MgO even with the low-spin $Fe^{2+}$
359 (Komabayashi et al. 2010) which would cause under-estimation of the pressure when an EoS
360 for MgO is applied. Figure 4 demonstrates that the data by Sata et al. (2010) at pressures
361 greater than 100 GPa show smaller volume of $Fe_3C$ compared with the EoS, which could be
362 due to the underestimation of pressure. The minor new peaks found during annealing in our
363 experiment are also consistent with $Fe_7C_3$, which appeared even at 29 GPa, indicating that
364 $Fe_7C_3$ in our experiments should have been formed by another mechanism, such as the
365 reaction between the sample and carbon contaminated from the diamond anvils. In addition,
366 our KCl pressure medium is insensitive to reaction with either this phase or hcp Fe.
367 Furthermore, the absence of Fe phases in our experiments indicates that reaction (1) did not
368 occur in the runs at 100 GPa.

369 The MGD model does not account for the anharmonic and electronic term in thermal
370 pressure, which may be significant for a metal under high temperature (e.g., Alfè et al. 2001). If
371 these two additional terms become significant at high temperatures, the $\alpha K_T$ value should show
372 a positive temperature dependence (Alfè et al. 2001). Figure 4b shows the misfit between the

data and model with a single $\alpha K_T$ value of 0.0068 GPa/K and there is no clear temperature dependence up to the highest temperature studied here. Therefore, the contributions from the anharmonic and electronic terms are minor in solid nonmagnetic $Fe_3C$, which justified the MGD model with only the vibrational thermal pressure term up to temperature conditions of Earth's core.

Our EoS for $Fe_3C$ is compared with reported volume data (Tateno et al. 2010; Hu et al. 2019; Liu et al. 2020). Fig. 5 shows calculated pressures from our EoS for the reported unit-cell volumes of $Fe_3C$ in Tateno et al. (2010) at 300 GPa. Note that their experimental pressure values were recalculated using the EoS of Fe by Dewaele et al. (2006) which is consistent with the pressure scales adopted in this study. Although the effect of carbon present in the hcp phase on the calculated pressure values is unknown (Tateno et al. 2010), the EoS for $Fe_3C$ constructed in this study give fairly consistent pressures with Tateno et al. (2010), which validates the applicability of our thermal EoS even at the inner core conditions. Our EoS for $Fe_3C$ is also consistent with shock Hugoniot data at subsolidus conditions (Hu et al. 2019) (Table 4). As discussed later in more detail, the melting temperature of $Fe_3C$ under high pressures is uncertain, but the P-T conditions up to 132.5 GPa and 2185 K in Hu et al. (2019) are well below the melting points (Mashino et al. 2019) and the conditions above 208.6 GPa and 4320 K are above the solidus (Takahashi et al. 2020). At the P-T conditions above the solidus, our EoS gives slightly larger density than Hu et al. (2019)'s data in partially or fully molten field, which is reasonable. A more recent shock wave experiment by Liu et al. (2020) reported density data of $Fe_3C$ consistent with Hu et al., (2019) and therefore should be consistent with our EoS.

**Stability of $Fe_3C$ under core pressures and temperatures**

Figure 6a shows calculated phase boundary for reaction (1) together with existing reports on phase relations of the system Fe-C (Tateno et al. 2010; Liu et al. 2016; Mashino et al. 2019; Takahashi et al., 2020). We estimated the uncertainty bounds from the propagated uncertainty in the EoS parameters for $Fe_3C$ constructed in this study. The reaction has a very steep positive Clapeyron slope with about 81 MPa/K at 87 GPa and 300 K and 47 MPa/K at 251 GPa and 3000 K.

The P-T location of reaction (1) is affected by the solubility of carbon in hcp Fe, which would move the boundary towards the low pressure side. It is well known that Fe phases accommodate up to 1-2 wt% carbon in the system Fe-C (Fei and Brosh 2014; Mashino et al. 2019). We make a simple calculation here to evaluate its effect. The location of reaction (1) with a reduced iron activity is calculated on the basis of Raoult's Law, namely ideal mixing. Raoult's Law would hold when the concentration of solute is low, and we assume here 2.3 wt% carbon solubility in hcp iron (10 mol% C). The results demonstrate that the boundary is shifted only by 1-4 GPa towards the low pressure side (light blue in Fig. 6a).

Reaction (1) was examined by *ab initio* methods at T = 0 (Mookherjee et al. 2011b). In contrast to our results, in their calculations, $Fe_3C$ phase was stable and reaction (1) does not occur over the entire core pressure range. The discrepancy between this study and Mookherjee et al. (2011b) can be attributed to the over-estimation of bulk modulus for iron-carbides using ab initio methods. We made precise calculations based on the EoS for each phase against a consistent pressure scale as discussed above.

Tateno et al. (2010) observed the formation of $Fe_3C$ phase in their Fe sample by in-situ XRD at about 340 GPa upon laser heating, which they attributed to contamination by carbon from the diamond anvils. While the details of the carbon transportation mechanism and the achievement of equilibrium between the Fe sample and incoming C are not known, the P-T condition of the first appearance of $Fe_3C$ at 5520 K and 344 GPa is consistent with

that of reaction (1) (Fig. 6b). Note that the unit-cell volume data for $Fe_3C$ by Tateno et al. (2010) discussed in Fig. 5 were collected after it was first synthesized at 5520 K and therefore the P-T conditions shown in Fig. 5 may not be relevant to the discussion of its stability. More recent in-situ XRD experiments confirmed the stability of $Fe_3C$ at high pressures (Takahashi et al. 2020). Most of their data up to 250 GPa are plotted consistently with reaction (1) in this study (Fig. 6b). Although they also claimed the stability of $Fe_3C$ above 300 GPa up to 1500 K (Fig. 6b), we consider it to be uncertain because the diffraction patterns were not clear enough to resolve peaks from $Fe_3C$ (Takahashi et al. 2020). In addition, Mashino et al. (2019), reported stability of $Fe_3C$ to 255 GPa at 3750 K as a subsolidus phase, based on textural observations of recovered samples. Although they did not identify the reaction in-situ, what they observed implies the assemblage of an invariant point where Fe, $Fe_3C$, $Fe_7C_3$ and liquid phases are stable. This invariant point forms at the intersection of reaction 1 and the eutectic reaction of $Fe+Fe_3C$ = liquid. The P-T location of the invariant point in Mashino et al. (2019) is consistent with reaction (1) calculated in this study (Fig. 6b).

The calculated boundary of reaction (1) shows that $Fe_3C$ is stable above 1140 K at 150 GPa, which contradicts the earlier laser-heated DAC experiments (Liu et al. 2016) who reported the reaction would be rather temperature independent at 150 GPa. Liu et al. (2016) conducted in-situ XRD experiments for the determination of the phase relations. A possible reconciliation of Liu et al. (2016)'s observations is metastable survival of the lower temperature assemblage at higher temperatures. In their in-situ experiments, $Fe + Fe_7C_3$ could have been first synthesized at lower temperatures above 150 GPa and they could have survived to higher temperatures after crossing the boundary of reaction (1) (Fig. 6a).

In summary, the calculated P-T locations of reaction (1) define the high-pressure stability of $Fe_3C$ and are consistent with most other experimental data (Tateno et al. 2010;

447 Mashino et al. 2019; Takahashi et al. 2020), and provide a possible explanation for the
448 misjudgment of phase stability in Liu et al. (2016).

449 The high-temperature stability of $Fe_3C$ is defined by the melting reaction: $Fe_3C$ =
450 $Fe_7C_3$+liquid. As described above, the eutectic curve of Fe+$Fe_3C$ determined by Mashino et
451 al. (2019) intersects with reaction (1) to form an invariant point (Fig. 6c). From the invariant
452 point, two other reactions originate: $Fe_3C$=$Fe_7C_3$+liquid and Fe+$Fe_7C_3$=liquid. Thus, the
453 invariant point defines the high-temperature limit of the stability of $Fe_3C$. Fig. 6c shows two
454 possible cases for the P-T location of the invariant point: an XRD analysis-based model
455 (Tateno et al. 2010; Takahashi et al. 2020) and a texture analysis-based model (Mashino et al.
456 2019). Tateno et al. (2010) observed the formation of $Fe_3C$ at 344 GPa and 5520 K, which is
457 a much higher temperature than Mashino et al. (2019)'s data. This P-T condition is consistent
458 with the extrapolated reaction of $Fe_3C$=$Fe_7C_3$+liquid constrained by another in-situ XRD
459 study (Takahashi et al. 2020). As both models are consistent with reaction (1) calculated in
460 this study, we cannot exclude either of them. A promising approach is to construct a
461 thermodynamic model for the system Fe-C including liquids and calculate the reactions
462 above, in order to distinguish the model with the correct invariant point.

463 Fig. 6c shows possible phase diagrams for the system Fe-C based on experimental
464 data (XRD or textural analysis) and our thermodynamic calculations. If the XRD-based
465 model is the case, $Fe_3C$ is stable over the outer core pressure conditions and the Fe-$Fe_3C$
466 subsystem may be relevant for an outer core composition near the eutectic point. In contrast,
467 if the invariant point constrained by the textural analysis of DAC experiments (Mashino et al.
468 2019) is the case, the subsolidus system would be Fe-$Fe_7C_3$.
469
470
471

This is the peer-reviewed, final accepted version for American Mineralogist, published by the Mineralogical Society of America.
The published version is subject to change. Cite as Authors (Year) Title. American Mineralogist, in press.
DOI: https://doi.org/10.2138/am-2021-7581. http://www.minsocam.org/

## IMPLICATIONS

The crystallizing sequence of an iron-alloy liquid at the outer core-inner core boundary (ICB) conditions is important because the crystallizing phase (liquidus phase) forms the inner core. Here we discuss two possible crystallizing scenarios: an XRD analysis-based model and a texture analysis-based model. We compare their resulting liquidus phases with seismological observations for the inner core (PREM, Dziewonski and Anderson 1981). For simplicity and to highlight the difference between the models, we assume the carbon content in the outer core to be slightly more than that of the eutectic point at 1.5 wt% (Fei and Brosh 2014), so that the liquidus phases at the ICB would be $Fe_3C$ (XRD analysis-based model) or $Fe_7C_3$ (texture analysis-based model). The liquidus temperature is assumed to be the same as for the eutectic temperature since the model considered here assumes an outer core composition close to the eutectic point. This assumption gives the lower bound of the liquidus temperature and therefore the upper bound in the calculated density of the liquidus phase: 5300 K for the XRD model and 3700 K for the texture model (Fig. 6c) with a fairly large uncertainty on the order of 500 K.

The XRD analysis-based model (Fig. 6c) suggests that the outer core would precipitate $Fe_3C$ to form the inner core at 5300 K. Figure 7 shows calculated density profiles of $Fe_3C$ at 300 K and 5300 $\pm$ 500 K based on the EoS constructed in this study. Even the 300 K density is smaller than the PREM density for the inner core and therefore $Fe_3C$ cannot account for the inner core.

The texture analysis-based model (Fig. 6c) suggests that the liquidus phase of the assumed outer core would be $Fe_7C_3$ at 3700 $\pm$ 500 K. Figure 7 shows a calculated density profile of $Fe_7C_3$ over the inner core pressure range based on the EoS constructed in Nakajima et al. (2011) which was used in the thermodynamic calculations in this study. As discussed in Nakajima et al. (2011), the density of $Fe_7C_3$ at 3700 K reasonably matches the inner core

density. Therefore, the system Fe-C may be relevant to the Earth's core if the core temperature is as low as 3700 K ± 500 K. On the other hand, such an outer core would result in a very low core-mantle boundary temperature (Nomura et al. 2014).

In conclusion, we have developed a subsolidus thermodynamic model of the system Fe-C with a newly constructed thermal EoS for $Fe_3C$. Based on the model, we inferred two possible melting relationships for the carbon-bearing core and found that the discrepancy in experimental results between Tateno et al. (2010) and Mashino et al. (2019) on the stability of $Fe_3C$ is critically important for the relevance of carbides in the inner core. A thermodynamic model for the melting relations in the Fe-C system needs to be established to address this issue in the near future.

Acknowledgements and Funding

We thank Z. Zhang for helpful advice in synthesis of stoichiometric $Fe_3C$. Portions of this work were performed at GeoSoilEnviroCARS (The University of Chicago, Sector 13), Advanced Photon Source (APS), Argonne National Laboratory (experiment 207783). GeoSoilEnviroCARS is supported by the National Science Foundation – Earth Sciences (EAR – 1634415) and Department of Energy- GeoSciences (DE-FG02-94ER14466). This research used resources of the Advanced Photon Source, a U.S. Department of Energy (DOE) Office of Science User Facility operated for the DOE Office of Science by Argonne National Laboratory under Contract No. DE-AC02-06CH11357. Two anonymous reviewers are acknowledged for their critical and constructive comments which improved the quality of the manuscript. This work is supported by the European Research Council (ERC) Consolidator Grant to T.K. (No. 647723).

## References

Alfè, D., Price, G. D., and Gillan, M. J. (2001) Thermodynamics of hexagonal-close-packed iron under Earth's core conditions. *Physical Review B*, *64*, 045123.

Anderson, O. L., Oda, H., and Isaak, D. (1992) A model for the computation of thermal expansivity at high compression and high temperatures: MgO as an example. *Geophysical Research Letters*, *19*, 1987-1990.

Aprilis, G., Kantor, I., Kupenko, I., Cerantola, V., Pakhomova, A., Collings, I.E., Torchio, R., Fedotenko, T., Chariton, S., Bykov, A., Bykova, E., Koemets, E., Vasiukov, D.M., McCammon, C., Dubrovinsky, L. and Dubrovinskaia, N (2019) Comparative study of the influence of pulsed and continuous wave laser heating on the mobilization of carbon and its chemical reaction with iron in a diamond anvil cell. *Journal of Applied Physics*, *125*, 095901.

Campbell, A.J., Danielson, L., Righter, K., Seagle, C.T., Wang, Y. and Prakapenka, V.B. (2009) High pressure effects on the iron–iron oxide and nickel–nickel oxide oxygen fugacity buffers. *Earth and Planetary Science Letters*, *286*, 556-564.

Chen, B., Li, Z., Zhang, D., Liu, J., Hu, M. Y., Zhao, J., Bi, W., Alp, E.E., Xiao, Y., Chow, P. and Li, J. (2014) Hidden carbon in Earth's inner core revealed by shear softening in dense Fe7C3. *Proceedings of the National Academy of Sciences*, *111*, 17755-17758.

Chen, B., Lai, X., Li, J., Liu, J., Zhao, J., Bi, W., Alp, E.E., Hu, M.Y. and Xiao, Y. (2018) Experimental constraints on the sound velocities of cementite Fe3C to core pressures. *Earth and Planetary Science Letters*, *494*, 164-171.

Dasgupta, R., Chi, H., Shimizu, N., Buono, A. S., and Walker, D. (2013) Carbon solution and partitioning between metallic and silicate melts in a shallow magma ocean: Implications for the origin and distribution of terrestrial carbon. *Geochimica et Cosmochimica Acta*, *102*, 191-212.

Dewaele, A., Loubeyre, P., Occelli, F., Mezouar, M., Dorogokupets, P. I., and Torrent, M. (2006) Quasihydrostatic equation of state of iron above 2 Mbar. *Physical Review Letters*, *97*, 215504.

Duman, E., Acet, M., Hülser, T., Wassermann, E. F., Rellinghaus, B., Itié, J. P., and Munsch, P. (2004) Large spontaneous magnetostrictive softening below the Curie temperature of Fe 3 C Invar particles. *Journal of Applied Physics*, *96*, 5668-5672.

Dziewonski, A. M., & Anderson, D. L. (1981). Preliminary reference Earth model. *Physics of the earth and planetary interiors*, *25*(4), 297-356.

551 Fei, Y. and Brosh, E. (2014) Experimental study and thermodynamic calculations of phase relations in the
552 Fe–C system at high pressure. *Earth and Planetary Science Letters*, *408*, 155-162.
553 Fei, Y., Zhang, L., Corgne, A., Watson, H., Ricolleau, A., Meng, Y., & Prakapenka, V. (2007) Spin
554 transition and equations of state of (Mg, Fe) O solid solutions. *Geophysical Research Letters*, *34*.
555 Fei, Y., Murphy, C., Shibazaki, Y., Shahar, A., and Huang, H. (2016) Thermal equation of state of hcp-iron:
556 Constraint on the density deficit of Earth's solid inner core. *Geophysical Research Letters*, *43*, 6837-6843.
557 Gao, L., Chen, B., Wang, J., Alp, E. E., Zhao, J., Lerche, M., Sturhahn, W., Scott H.P, Huang, F., Ding, Y.,
558 Sinogeikin, S.V., Lundstrom, C.C., Bass, J.D., and Li, J (2008) Pressure-induced magnetic transition and
559 sound velocities of Fe3C: Implications for carbon in the Earth's inner core. *Geophysical Research*
560 *Letters*, *35*.
561 Gao, L., Chen, B., Zhao, J., Alp, E. E., Sturhahn, W. and Li, J. (2011) Effect of temperature on sound
562 velocities of compressed Fe3C, a candidate component of the Earth's inner core. *Earth and Planetary*
563 *Science Letters*, *309*(3-4), 213-220.
564 Hallstedt, B., Djurovic, D., von Appen, J., Dronskowski, R., Dick, A., Körmann, F., Hickel, T., and
565 Neugebauer, J. (2010). Thermodynamic properties of cementite (Fe3C). *Calphad*, *34*(1), 129-133.
566 Hirose, K., Labrosse, S. and Hernlund, J. (2013) Composition and state of the core. *Annual Review of Earth*
567 *and Planetary Sciences*, *41*, 657-691.
568 Hu, X., Fei, Y., Yang, J., Cai, Y., Ye, S., Qi, M., Liu, F. and Zhang, M. (2019) Phase stability and thermal
569 equation of state of iron carbide Fe3C to 245 GPa. *Geophysical Research Letters*, *46*, 11018-11024.
570 Jackson, I. and Rigden, S.M. (1996) Analysis of PVT data: constraints on the thermoelastic properties of
571 high-pressure minerals. *Physics of the earth and planetary interiors*, *96*, 85-112.
572 Komabayashi, T., Hirose, K., Nagaya, Y., Sugimura, E., & Ohishi, Y. (2010). High-temperature
573 compression of ferropericlase and the effect of temperature on iron spin transition. *Earth and Planetary*
574 *Science Letters*, *297*(3-4), 691-699.
575 Komabayashi, T. (2014) Thermodynamics of melting relations in the system Fe-FeO at high pressure:
576 Implications for oxygen in the Earth's core. *Journal of Geophysical Research: Solid Earth*, *119*,
577 4164-4177.

578 Kuwayama, Y., Morard, G., Nakajima, Y., Hirose, K., Baron, A. Q., Kawaguchi, S. I., Tsuchiya, T.,
579 Ishikawa, D., Hirao, N., and Ohishi, Y. (2020) Equation of State of Liquid Iron under Extreme
580 Conditions. *Physical Review Letters*, *124*, 165701.
581 Lai, X., Zhu, F., Liu, J., Zhang, D., Hu, Y., Finkelstein, G. J., Dera, P. and Chen, B. (2018) The high-pressure
582 anisotropic thermoelastic properties of a potential inner core carbon-bearing phase, Fe7C3, by
583 single-crystal X-ray diffraction. *American Mineralogist: Journal of Earth and Planetary Materials*, *103*,
584 1568-1574.
585 Li, J., Mao, H. K., Fei, Y., Gregoryanz, E., Eremets, M., and Zha, C. S. (2002) Compression of Fe3C to 30
586 GPa at room temperature. *Physics and Chemistry of Minerals*, *29*, 166-169.
587 Lin, J.F., Struzhkin, V.V., Mao, H.K., Hemley, R.J., Chow, P., Hu, M.Y. and Li, J. (2004) Magnetic
588 transition in compressed Fe 3 C from X-ray emission spectroscopy. *Physical Review B*, *70*, 212405.
589 Liu, J., Lin, J.F., Prakapenka, V.B., Prescher, C. and Yoshino, T. (2016) Phase relations of Fe3C and Fe7C3
590 up to 185 GPa and 5200 K: Implication for the stability of iron carbide in the Earth's core. *Geophysical*
591 *Research Letters*, *43*, 12-415.
592 Liu, X., Fan, L., Yang, G., Chen, X., and Huang, H. (2020) Hugoniot equation of state of cementite (Fe3C)
593 up to 250 GPa and its geophysical implications. *Physics of the Earth and Planetary Interiors*, 106506.
594 Litasov, K.D., Sharygin, I.S., Dorogokupets, P.I., Shatskiy, A., Gavryushkin, P.N., Sokolova, T. S., Ohtani,
595 E., Li, J. and Funakoshi, K. (2013) Thermal equation of state and thermodynamic properties of iron
596 carbide Fe3C to 31 GPa and 1473 K. *Journal of Geophysical Research: Solid Earth*, *118*, 5274-5284.
597 Litasov, K.D., Rashchenko, S.V., Shmakov, A.N., Palyanov, Y.N. and Sokol, A.G. (2015) Thermal
598 expansion of iron carbides, Fe7C3 and Fe3C, at 297–911 K determined by in situ X-ray
599 diffraction. *Journal of Alloys and Compounds*, *628*, 102-106.
600 Lord, O. T., Walter, M. J., Dasgupta, R., Walker, D. and Clark, S.M. (2009) Melting in the Fe–C system to
601 70 GPa. *Earth and Planetary Science Letters*, *284*, 157-167.
602 Mashino, I., Miozzi, F., Hirose, K., Morard, G. and Sinmyo, R. (2019) Melting experiments on the Fe–C
603 binary system up to 255 GPa: Constraints on the carbon content in the Earth's core. *Earth and Planetary*
604 *Science Letters*, *515*, 135-144.

McCammon, C., Bureau, H., Cleaves II, H.J., Cottrell, E., Dorfman, S.M., Kellogg, L.H., Li, J., Mikhail, S., Moussalam, Y., Sanloup, C., Thomson, A. R. and Brovarone, A.V. (2020) Deep Earth carbon reactions through time and space. *American Mineralogist*, *105*, 22-27.

McDonough, W.F. and Sun, S.S. (1995) The composition of the Earth. *Chemical geology*, *120*, 223-253.

Mookherjee, M. (2011a) Elasticity and anisotropy of $Fe_3C$ at high pressures. *American Mineralogist*, *96*, 1530-1536.

Mookherjee, M., Nakajima, Y., Steinle-Neumann, G., Glazyrin, K., Wu, X., Dubrovinsky, L., McCammon, C. and Chumakov, A. (2011b) High-pressure behavior of iron carbide ($Fe_7C_3$) at inner core conditions. *Journal of Geophysical Research: Solid Earth*, *116*(B4).

Morard, G., Andrault, D., Antonangeli, D., Nakajima, Y., Auzende, A.L., Boulard, E., Servera, S., Clark, A., Lord, O.T., Seibert, J., Svitlyk, V., Garbarino, G., and Mezouar, M (2017) Fe–FeO and Fe–Fe3C melting relations at Earth's core–mantle boundary conditions: Implications for a volatile-rich or oxygen-rich core. *Earth and Planetary Science Letters*, *473*, 94-103.

Nakajima, Y., Takahashi, E., Suzuki, T. and Funakoshi, K.I. (2009) "Carbon in the core" revisited. *Physics of the Earth and Planetary Interiors*, *174*, 202-211.

Nakajima, Y., Takahashi, E., Sata, N., Nishihara, Y., Hirose, K., Funakoshi, K. I. and Ohishi, Y. (2011) Thermoelastic property and high-pressure stability of Fe7C3: Implication for iron-carbide in the Earth's core. *American Mineralogist*, *96*, 1158-1165.

Noguchi, M., Komabayashi, T., Hirose, K., and Ohishi, Y. (2013) High-temperature compression experiments of CaSiO 3 perovskite to lowermost mantle conditions and its thermal equation of state. *Physics and Chemistry of Minerals*, *40*, 81-91.

Nomura, R., Hirose, K., Uesugi, K., Ohishi, Y., Tsuchiyama, A., Miyake, A., & Ueno, Y. (2014) Low core-mantle boundary temperature inferred from the solidus of pyrolite. *Science*, *343*, 522-525.

Ono, S. and Mibe, K. (2010) Magnetic transition of iron carbide at high pressures. *Physics of the Earth and Planetary Interiors*, *180*, 1-6.

Palme, H. and O'Neill, H.S.C. (2003) Cosmochemical estimates of mantle composition. *Treatise on geochemistry*, *2*, 568.

632 Prakapenka, V.B., Kubo, A., Kuznetsov, A., Laskin, A., Shkurikhin, O., Dera, P., Rivers, M.L. and Sutton,
633 S. R. (2008) Advanced flat top laser heating system for high pressure research at GSECARS: application
634 to the melting behavior of germanium. *High Pressure Research*, *28*, 225-235.
635 Prescher, C., Dubrovinsky, L., McCammon, C., Glazyrin, K., Nakajima, Y., Kantor, A., Merlini, M. and
636 Hanfland, M. (2012) Structurally hidden magnetic transitions in $Fe_3C$ at high pressures. *Physical Review*
637 *B*, *85*, 140402.
638 Prescher, C., Dubrovinsky, L., Bykova, E., Kupenko, I., Glazyrin, K., Kantor, A., McCammon, C.,
639 Mookherjee, M., Nakajima, Y., Miyajima, N., Sinmyo, R., Cerantola, V., Dubrovinskaia, N., Prakapenka,
640 V., Ruffer, R., Chumakov, A., and Hanfland, M. (2015) High Poisson's ratio of Earth's inner core
641 explained by carbon alloying. *Nature Geoscience*, *8*, 220-223.
642 Prescher, C. and Prakapenka, V.B. (2015) DIOPTAS: a program for reduction of two-dimensional X-ray
643 diffraction data and data exploration. *High Pressure Research*, *35*, 223-230.
644 Sata, N., Hirose, K., Shen, G., Nakajima, Y., Ohishi, Y. and Hirao, N. (2010) Compression of FeSi, Fe3C,
645 Fe0. 95O, and FeS under the core pressures and implication for light element in the Earth's core. *Journal*
646 *of Geophysical Research: Solid Earth*, *115*(B9).
647 Scott, H.P., Williams, Q. and Knittle, E. (2001) Stability and equation of state of Fe3C to 73 GPa:
648 Implications for carbon in the Earth's core. *Geophysical Research Letters*, *28*, 1875-1878.
649 Siebert, J., Corgne, A. and Ryerson, F.J. (2011) Systematics of metal–silicate partitioning for many
650 siderophile elements applied to Earth's core formation. *Geochimica et Cosmochimica Acta*, *75*,
651 1451-1489.
652 Sokolova, T. S., Dorogokupets, P. I., and Litasov, K. D. (2013) Self-consistent pressure scales based on the
653 equations of state for ruby, diamond, MgO, B2–NaCl, as well as Au, Pt, and other metals to 4 Mbar and
654 3000 K. *Russian Geology and Geophysics*, *54*, 181-199.
655 Solomatova, N.V., Caracas, R. and Manning, C.E. (2019) Carbon sequestration during core formation
656 implied by complex carbon polymerization. *Nature communications*, *10*, 1-7.
657 Steinle-Neumann, G., Stixrude, L. and Cohen, R.E. (1999) First-principles elastic constants for the hcp
658 transition metals Fe, Co, and Re at high pressure. *Physical Review B*, *60*, 791.
659 Takahashi, S., Ohtani, E., Sakai, T., Kamada, S., Ozawa, S., Sakamaki, T., Miyahara, M., Ito, Y., Hirao, N.,
660 and Ohishi, Y. (2020) Phase and melting relations of Fe3C to 300 GPa and carbon in the core. In Manning,

C., Lin, J.F., and Mao, W., Eds. Carbon in Earth's Interior, p 25-36 *Geophysical Monograph Series*, American Geophysical Union, Washington, DC.

Tateno, S., Hirose, K., Ohishi, Y., and Tatsumi, Y. (2010) The structure of iron in Earth's inner core. Science 330, 359-361.

Tateno, S., Komabayashi, T., Hirose, K., Hirao, N. and Ohishi, Y. (2019) Static compression of B2 KCl to 230 GPa and its PVT equation of state. *American Mineralogist*, *104*, 718-723.

Vinet, P., Ferrante, J., Rose, J.H. and Smith, J.R. (1987) Compressibility of solids. *Journal of Geophysical Research: Solid Earth*, *92*, 9319-9325.

Vočadlo, L., Brodholt, J., Dobson, D.P., Knight, K.S., Marshall, W.G., Price, G.D. and Wood, I. G. (2002) The effect of ferromagnetism on the equation of state of Fe3C studied by first-principles calculations. *Earth and Planetary Science Letters*, *203*, 567-575.

Walker, D., Li, J., Kalkan, B. and Clark, S.M. (2015) Thermal, compositional, and compressional demagnetization of cementite. *American Mineralogist*, *100*, 2610-2624.

Wood, B.J. (1993) Carbon in the core. *Earth and Planetary Science Letters*, *117*, 593-607.

Wood, I.G., Vočadlo, L., Knight, K.S., Dobson, D.P., Marshall, W.G., Price, G.D. and Brodholt, J. (2004) Thermal expansion and crystal structure of cementite, Fe3C, between 4 and 600 K determined by time-of-flight neutron powder diffraction. *Journal of Applied Crystallography*, *37*(1), 82-90.

Zhang, Z., Hastings, P., Von der Handt, A., & Hirschmann, M.M. (2018) Experimental determination of carbon solubility in Fe-Ni-S melts. *Geochimica et Cosmochimica Acta*, *225*, 66-79.

Figure Captions

Figure 1: Diffraction patterns at room temperature (quench) from 28 GPa to 117 GPa. Indices for orthorhombic (Pnma) $Fe_3C$ and B2 KCl are shown. The purple squares show selected reflections from $Fe_7C_3$ Nakajima et al., (2011).

Figure 2: Example diffraction patterns at 100 GPa and elevated temperature, compared with room temperature (quench). No new peaks are apparent upon quench and all peaks can be sufficiently indexed with $Fe_3C$, $Fe_7C_3$ and KCl. A LeBail fit of $Fe_7C_3$, $Fe_3C$ and KCl to the high temperature pattern is shown in light green solid line (1.7% Rwp). Indices are shown for the high temperature (HT) pattern. The thin black line is the misfit. The 2D cake (unrolled) XRD image at high temperature is also shown below the integrated patterns.

Figure 3: (a)The measured unit-cell volumes of $Fe_3C$ up to 117 GPa at room temperature are shown in the triangles. Where not visible, the errors in volume are smaller than the symbol. The filled diamonds are volumes from Sata et al (2010) at recalculated MgO pressure scale (Sokolova et al. 2013). The open symbols show previously measured volumes, also at room temperature: open squares (Litasov et al. 2013), open circles (Ono and Mibe 2010). The solid black line shows the best fit room temperature Vinet EoS. (b)The measured unit-cell volumes of $Fe_3C$ which were used for the fit to the thermal EoS, up to ~100 GPa and temperatures up to 2100 K, in addition to room temperature data, are shown in the triangles. The filled diamonds are volumes from Sata et al (2010). The fitted parameters are listed in Table 2. The corresponding isotherms at high temperature are shown in addition to the room temperature isotherm.

Figure 4: The misfit between the observed and the calculated pressure, based on our (a) MGD and (b) $\alpha K_T$ thermal EoS for $Fe_3C$. The blue circles are room temperature measurements. The squares and triangles show elevated temperature. The purple diamonds show data from Sata et al (2010). Note that the data above 100 GPa in Sata et al. (2010) were not used in the EoS fit.

Figure 5: Comparison of the pressures between the EoS constructed in this study and Tateno et al. (2010) for the unit-cell volumes of $Fe_3C$ obtained in Tateno et al. (2010)'s experiments.

Figure 6: (a) Phase relations in the Fe-C system up to 400 GPa and 6000K together with existing data (L16, Liu et al. 2016; M19, Mashino et al. 2019; T20, Takahashi et al. 2020). The solid red line shows reaction (1) calculated in this study with the uncertainties in the EoS of $Fe_3C$ (pale red) and in the carbon solubility in hcp Fe by 2.3 wt% (blue). (b) Selected experimental data points from the literature shown in the inset. Mashino et al. (2019) observed an invariant assemblage that implies the invariant point is an intersection of reaction 1 (this study) and the eutectic melting curve (green, Mashino et al. 2019). The black lines are the observed phase boundary by in-situ XRD by Liu et al. (2016). Experimental data of Takahashi et al. (2020) are plotted; their 300 K data are not shown. Tateno et al. (2010) observed the formation of $Fe_3C$ in Fe sample at 5520 K and 344 GPa. (c) Inferred phase diagram for the system Fe-C. The stars denote two cases of the invariant point where Fe, $Fe_3C$, $Fe_7C_3$, and liquid coexist. The in-situ XRD analysis-based work (Tateno et al. 2010; Takahashi et al. 2020) forms the invariant point at 360 GPa and 5500 K (blue star) whereas the texture analysis-based model (Mashino et al. 2019) placed it at 275 GPa and 3500 K (green star). A melting curve for pure Fe is taken from K14, Komabayashi (2014). Rxn, reaction.

731 Figure 7: The density versus pressure relation for the liquid outer core and solid inner core are
732 shown with PREM (blue circles) and candidate iron carbides. The pressure for the inner core
733 boundary (ICB) is indicated. Solid $Fe_3C$ is shown at 300 K and 5300 ± 500 K in the solid
734 orange line (this study). Solid $Fe_7C_3$ at 3700 ± 500 K is shown in the dot-dash line (Nakajima
735 et al., 2011). Solid hcp iron at 5800 K (Dewaele et al. 2006) is shown in the short-dash line.
736 The uncertainty bar attached to the density of $Fe_3C$ is propagated from the uncertainties in the
737 EoS parameters.

This is the peer-reviewed, final accepted version for American Mineralogist, published by the Mineralogical Society of America.
The published version is subject to change. Cite as Authors (Year) Title. American Mineralogist, in press.
DOI: https://doi.org/10.2138/am-2021-7581. http://www.minsocam.org/

Table 1. Experimental results of pressure-volume-temperature data for $Fe_3C$

| | P (GPa) | V of $Fe_3C$ ($Å^3$) | T (K) | a (Å) | b (Å) | c (Å) | V of KCl ($Å^3$) |
|---|---|---|---|---|---|---|---|
| Run #1 | 28.6(4) | 138.2(4) | 300 | 4.900(7) | 6.488(12) | 4.348(6) | 34.324(3) |
| | 45.4(3) | 131.9(4) | 300 | 4.831(7) | 6.397(12) | 4.269(5) | 30.898(2) |
| | 44.8(4) | 132.0(3) | 300 | 4.837(5) | 6.393(9) | 4.268(4) | 30.986(2) |
| | 52.4(14) | 129.9(3) | 300 | 4.814(7) | 6.353(11) | 4.246(6) | 29.833(7) |
| | 63.8(2) | 126.7(3) | 300 | 4.770(6) | 6.308(9) | 4.211(5) | 28.393(1) |
| Run #2 | 73.3(13) | 125.2(8) | 300 | 4.752(14) | 6.293(31) | 4.185(8) | 27.376(5) |
| | 86.5(19) | 121.7(6) | 300 | 4.726(12) | 6.223(22) | 4.138(6) | 26.188(6) |
| | 99.5(1) | 119.1(1) | 300 | 4.710(3) | 6.166(4) | 4.103(2) | 25.201(1) |
| | 98.8(9) | 119.4(6) | 300 | 4.694(13) | 6.190(25) | 4.111(7) | 25.249(3) |
| | 116.8(6) | 116.8(9) | 300 | 4.665(18) | 6.131(38) | 4.085(10) | 24.082(2) |
| Run #3 | 46.1(15) | 132.2(5) | 300 | 4.837(9) | 6.360(15) | 4.296(8) | 30.786(8) |
| | 53.8(5) | 129.5(7) | 300 | 4.829(9) | 6.316(27) | 4.246(9) | 29.643(3) |
| | 80.3(5) | 123.6(7) | 300 | 4.757(10) | 6.224(31) | 4.173(9) | 26.724(2) |
| Run #1 | 30.5(6) | 140.0(7) | 1380(88) | 4.923(13) | 6.501(22) | 4.376(10) | 34.604(5) |
| | 30.5(6) | 140.2(6) | 1370(98) | 4.929(11) | 6.514(19) | 4.366(9) | 34.604(5) |
| | 30.1(5) | 141.1(5) | 1436(111) | 4.945(10) | 6.538(17) | 4.363(8) | 34.755(5) |
| | 30.2(6) | 141.1(5) | 1460(90) | 4.946(10) | 6.541(17) | 4.360(8) | 34.730(5) |
| | 30.2(7) | 141.2(5) | 1491(105) | 4.953(10) | 6.543(16) | 4.358(7) | 34.773(6) |
| | 47.0(2) | 134.4(5) | 1501(87) | 4.877(10) | 6.441(18) | 4.278(7) | 31.179(1) |
| | 47.2(1) | 134.4(5) | 1515(69) | 4.877(10) | 6.441(18) | 4.278(7) | 31.156(1) |
| | 46.6(4) | 133.9(6) | 1545(69) | 4.866(11) | 6.423(20) | 4.284(9) | 31.266(3) |
| | 46.7(4) | 134.2(6) | 1603(79) | 4.876(12) | 6.422(21) | 4.286(9) | 31.280(2) |
| | 46.7(4) | 134.2(6) | 1633(67) | 4.876(12) | 6.422(21) | 4.286(9) | 31.293(2) |
| | 46.9(4) | 134.4(6) | 1686(71) | 4.879(12) | 6.421(21) | 4.288(9) | 31.280(2) |
| | 54.1(16) | 131.4(3) | 1395(89) | 4.832(6) | 6.373(8) | 4.269(4) | 30.020(8) |
| | 54.1(16) | 131.6(3) | 1407(76) | 4.835(7) | 6.375(10) | 4.269(5) | 30.020(8) |
| | 54.2(16) | 131.6(4) | 1424(116) | 4.835(8) | 6.381(11) | 4.268(6) | 30.020(8) |
| | 54.4(16) | 131.9(4) | 1487(47) | 4.838(8) | 6.382(12) | 4.270(7) | 30.020(8) |
| | 54.8(12) | 132.1(3) | 1568(62) | 4.842(7) | 6.388(10) | 4.270(6) | 29.989(6) |
| | 64.1(9) | 128.9(4) | 1495(94) | 4.799(8) | 6.351(12) | 4.230(6) | 28.747(4) |
| | 64.4(9) | 128.9(3) | 1549(52) | 4.804(7) | 6.345(11) | 4.229(6) | 28.726(4) |
| | 64.5(9) | 129.1(4) | 1580(39) | 4.797(9) | 6.350(13) | 4.237(7) | 28.726(4) |
| | 64.8(10) | 129.1(4) | 1630(48) | 4.797(9) | 6.350(13) | 4.237(7) | 28.704(4) |
| | 64.9(10) | 129.2(4) | 1661(41) | 4.801(9) | 6.352(13) | 4.235(7) | 28.704(4) |
| | 65.2(8) | 129.3(3) | 1709(39) | 4.802(7) | 6.349(11) | 4.240(6) | 28.689(4) |
| | 65.2(10) | 129.3(3) | 1737(38) | 4.802(7) | 6.349(11) | 4.240(6) | 28.695(4) |
| | 65.1(14) | 129.3(3) | 1786(41) | 4.802(7) | 6.349(11) | 4.240(6) | 28.725(6) |

This is the peer-reviewed, final accepted version for American Mineralogist, published by the Mineralogical Society of America.
The published version is subject to change. Cite as Authors (Year) Title. American Mineralogist, in press.
DOI: https://doi.org/10.2138/am-2021-7581. http://www.minsocam.org/

| | | | | | | | |
|---|---|---|---|---|---|---|---|
| | 65.7(12) | 129.5(3) | 1834(41) | 4.805(7) | 6.349(11) | 4.245(6) | 28.670(5) |
| | 66.1(6) | 129.6(3) | 1904(40) | 4.813(6) | 6.347(8) | 4.241(4) | 28.645(3) |
| | 66.4(9) | 129.6(3) | 1964(44) | 4.814(6) | 6.347(9) | 4.241(5) | 28.633(4) |
| | 66.2(10) | 129.6(2) | 1995(45) | 4.818(5) | 6.352(7) | 4.236(4) | 28.670(5) |
| | 66.4(13) | 129.8(3) | 2059(45) | 4.823(6) | 6.351(8) | 4.237(4) | 28.664(6) |
| Run #2 | 74.4(11) | 126.7(7) | 1692(26) | 4.775(14) | 6.321(30) | 4.196(7) | 27.662(4) |
| | 74.5(11) | 127.0(8) | 1741(25) | 4.778(15) | 6.333(33) | 4.197(8) | 27.662(4) |
| | 74.9(9) | 126.9(8) | 1791(26) | 4.783(15) | 6.318(34) | 4.201(8) | 27.641(4) |
| | 89.9(14) | 123.1(5) | 1661(47) | 4.757(10) | 6.229(22) | 4.154(6) | 26.229(5) |
| | 90.2(16) | 123.0(6) | 1734(43) | 4.748(12) | 6.241(25) | 4.151(6) | 26.214(5) |
| | 90.0(24) | 122.9(4) | 1788(45) | 4.749(7) | 6.231(15) | 4.154(4) | 26.250(8) |
| | 90.9(16) | 122.8(5) | 1850(53) | 4.746(10) | 6.231(20) | 4.153(5) | 26.188(6) |
| | 100.3(7) | 120.2(1) | 1358(44) | 4.717(3) | 6.193(5) | 4.115(2) | 25.351(2) |
| | 101.2(16) | 120.2(1) | 1406(30) | 4.717(3) | 6.193(5) | 4.115(2) | 25.294(5) |
| | 101.4(16) | 120.2(1) | 1455(33) | 4.721(2) | 6.188(4) | 4.114(2) | 25.294(5) |
| | 101.6(16) | 120.3(2) | 1528(33) | 4.720(4) | 6.190(6) | 4.119(3) | 25.294(5) |
| | 101.7(16) | 120.4(2) | 1564(37) | 4.724(4) | 6.190(6) | 4.118(3) | 25.294(5) |
| | 101.9(16) | 120.5(1) | 1626(42) | 4.729(3) | 6.189(5) | 4.118(2) | 25.294(5) |
| Sata et al. (2010)[a] | | | | | | | |
| | 50.25(59) | 130.804(30) | 300 | 4.24773(68) | 4.83204(79) | 6.35837(64) | |
| | 69.77(38) | 125.238(30) | 300 | 4.18121(76) | 4.77308(78) | 6.27259(63) | |
| | 77.95(38) | 124.076(30) | 300 | 4.16139(77) | 4.75747(69) | 6.2672(15) | |
| | 101.57(45) | 119.583(33) | 300 | 4.11026(80) | 4.70626(90) | 6.1819(16) | |

[a] Pressure values were recalculated using MgO pressure scale by Sokolova et al. (2013).

This is the peer-reviewed, final accepted version for American Mineralogist, published by the Mineralogical Society of America.
The published version is subject to change. Cite as Authors (Year) Title. American Mineralogist, in press.
DOI: https://doi.org/10.2138/am-2021-7581. http://www.minsocam.org/

Table 2. Equation of state parameters for $Fe_3C$.

| | | | | | | MGD | | | $\alpha K_T$ | Anderson-Grüneisen[a] | | |
|---|---|---|---|---|---|---|---|---|---|---|---|---|
| Material | | EoS[b] | $V_0$ (Å$^3$) | $K_0$ (GPa) | $K'_0$ | $\gamma_0$ | q | $\theta_0$ (K) | $\alpha K_T$ (GPa/K) | $\alpha_0$ (*$10^{-5}$/K) | $\delta$ | $\kappa$ |
| $Fe_3C$ | This study | V | 151.6(12) | 232(24) | 5.09(46) | 2.3(3) | 3.4(9) | 407(fixed) | | 5.6 | 7.4 | 0.2 |
| | | V | 152(fixed) | 232(fixed) | 5.1(fixed) | | | | 0.0068(2) | | | |
| | Litasov et al. (2013) | BM | 154.6(1) | 192(3) | 4.5(1) | 2.09(4) | -0.1(3) | 490(120) | | | | |
| $Fe_7C_3$ | Nakajima et al. (2011) | BM | 184.2(3) | 253(7) | 3.6(2) | 2.57(5) | 2.2(5) | 920(140) | | | | |
| | | V[c] | 183.9(2) | 257(6) | 3.7(2) | 2.49(5) | 2.9(4) | 665 (fixed) | | 5.2 | 5.4 | -0.1 |
| hcp Fe[d] | Dewaele et al. (2006) | V | 22.428(98) | 163.4(7.9) | 5.38(16) | | | | | 5.8 | 5.1 | 1.4 |

[a] AG model parameters were obatined by fitting to P-V-T data produced from the MGD model.

[b] V, Vinet EoS; BM, Birch-Murnaghan EoS.

[c] The experimental pressure values were recalcuated based on the MgO pressure scale of Sokolova et al. (2013).

[d] The MGD parameters are not shown as Dewaele et al. (2006) used a different formulation.

This is the peer-reviewed, final accepted version for American Mineralogist, published by the Mineralogical Society of America.
The published version is subject to change. Cite as Authors (Year) Title. American Mineralogist, in press.
DOI: https://doi.org/10.2138/am-2021-7581. http://www.minsocam.org/

Table 3. Gibbs energies of phases at 1 bar, T ($J \cdot mol^{-1}$)

| Phase | |
|---|---|
| hcp iron[a] | $G(P_0,T) = 12460.921+386.99162*T-52.2754*T*lnT+0.000177578*T^{2}-395355*T^{-1}-2476.28*T^{0.5}$ |
| $Fe_3C$[b] | $G(P_0,T) = -10195.861+690.9499*T-118.4764*T*lnT-0.0007*T^{2}+590527*T^{-1}$ |
| $Fe_7C_3$[c] | $G(P_0,T) = 32848.53-12.506*T+30*RT*ln(1-exp(-455/T))+47*T*ln(1-exp(-200/T))$ |

[a] hcp iron: Komabayashi (2014).

[b] $Fe_3C$: Hallstedt et al. (2010)

[c] $Fe_7C_3$: Fei and Brosh (2014)

This is the peer-reviewed, final accepted version for American Mineralogist, published by the Mineralogical Society of America.
The published version is subject to change. Cite as Authors (Year) Title. American Mineralogist, in press.
DOI: https://doi.org/10.2138/am-2021-7581. http://www.minsocam.org/

Table 4. Comparison of the density of $Fe_3C$ with Hugoniot data.

| P (GPa)[a] | 85.6 | 132.5 | 171.6 | 208.6 | 227.5 | 245 | |
|---|---|---|---|---|---|---|---|
| T (K)[a] | 1190 | 2185 | 3210 | 4320 | 4928 | 5530 | |
| Density ($g/cm^3$) | 9.655(23)[b] | 10.270(61)[b] | 10.637(50) | 10.951(83)[c] | 11.110(55)[c] | 11.155(61)[c] | Hugoniot (Hu et al. 2019) |
| | 9.675 | 10.317 | 10.777 | 11.170 | 11.358 | 11.525 | EoS (This study) |

[a] The P-T conditions are from the Hugoniot (Hu et al. 2019).

[b] Subsolidus data.

[c] Super solidus data.

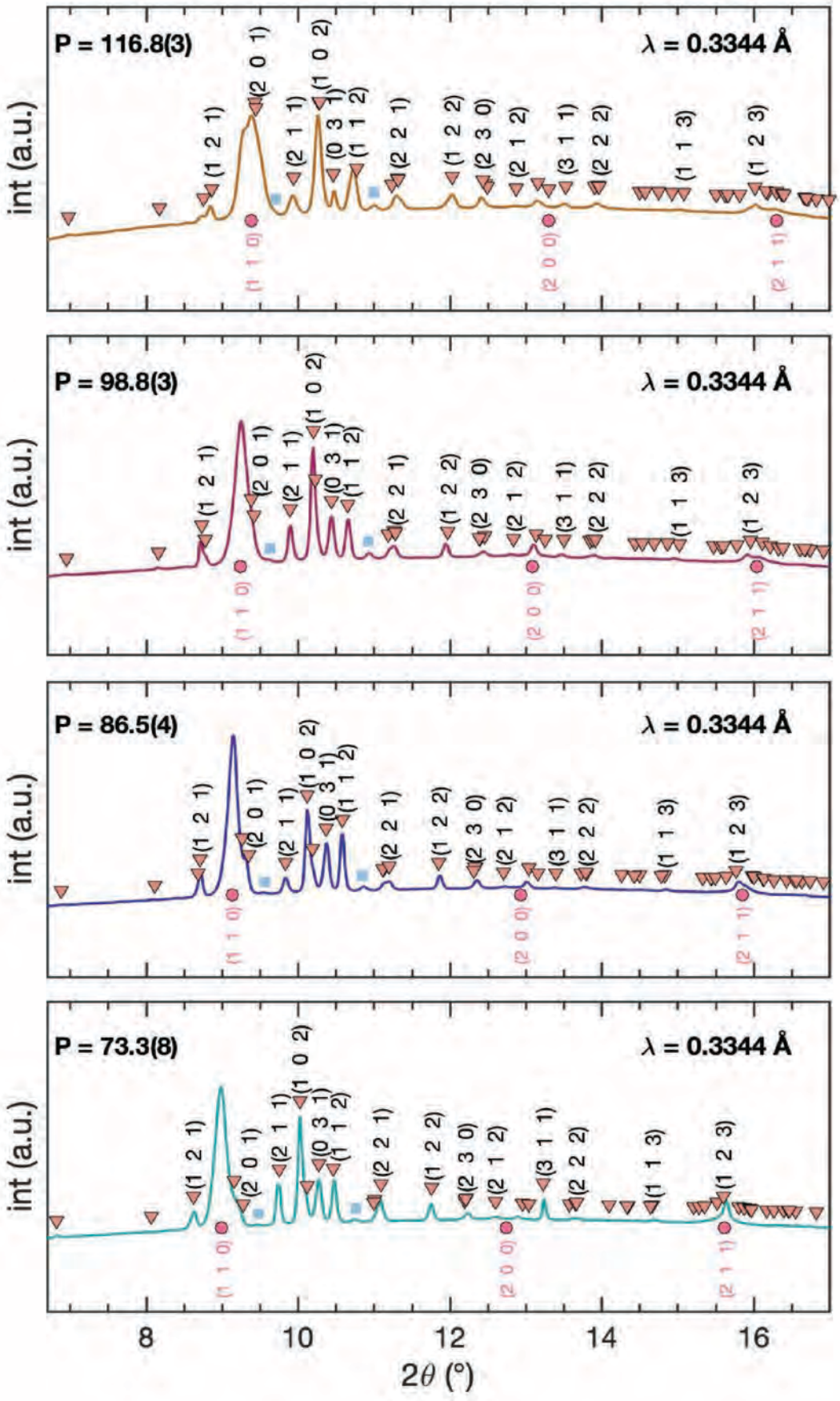
P = 116.8(3)
λ = 0.3344 Å
P = 98.8(3)
λ = 0.3344 Å
P = 86.5(4)
λ = 0.3344 Å
P = 73.3(8)
λ = 0.3344 Å
int (a.u.)
2θ (°)
8
10
12
14
16

Figure 1

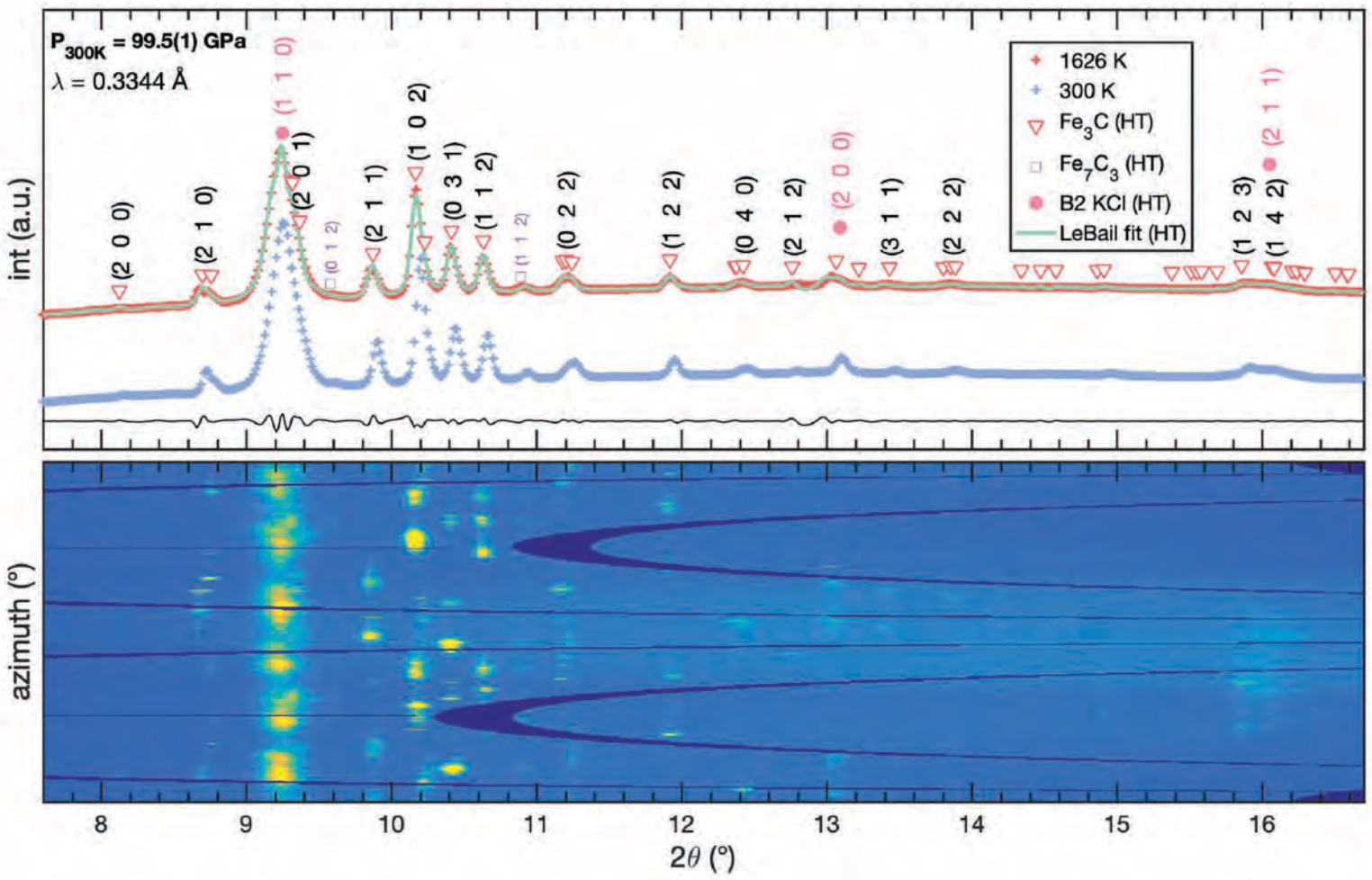
P300K = 99.5(1) GPa
λ = 0.3344 Å
1626 K
300 K
Fe3C (HT)
Fe7C3 (HT)
B2 KCl (HT)
LeBail fit (HT)
int (a.u.)
azimuth (°)
2θ (°)
8
9
10
11
12
13
14
15
16

Figure 2

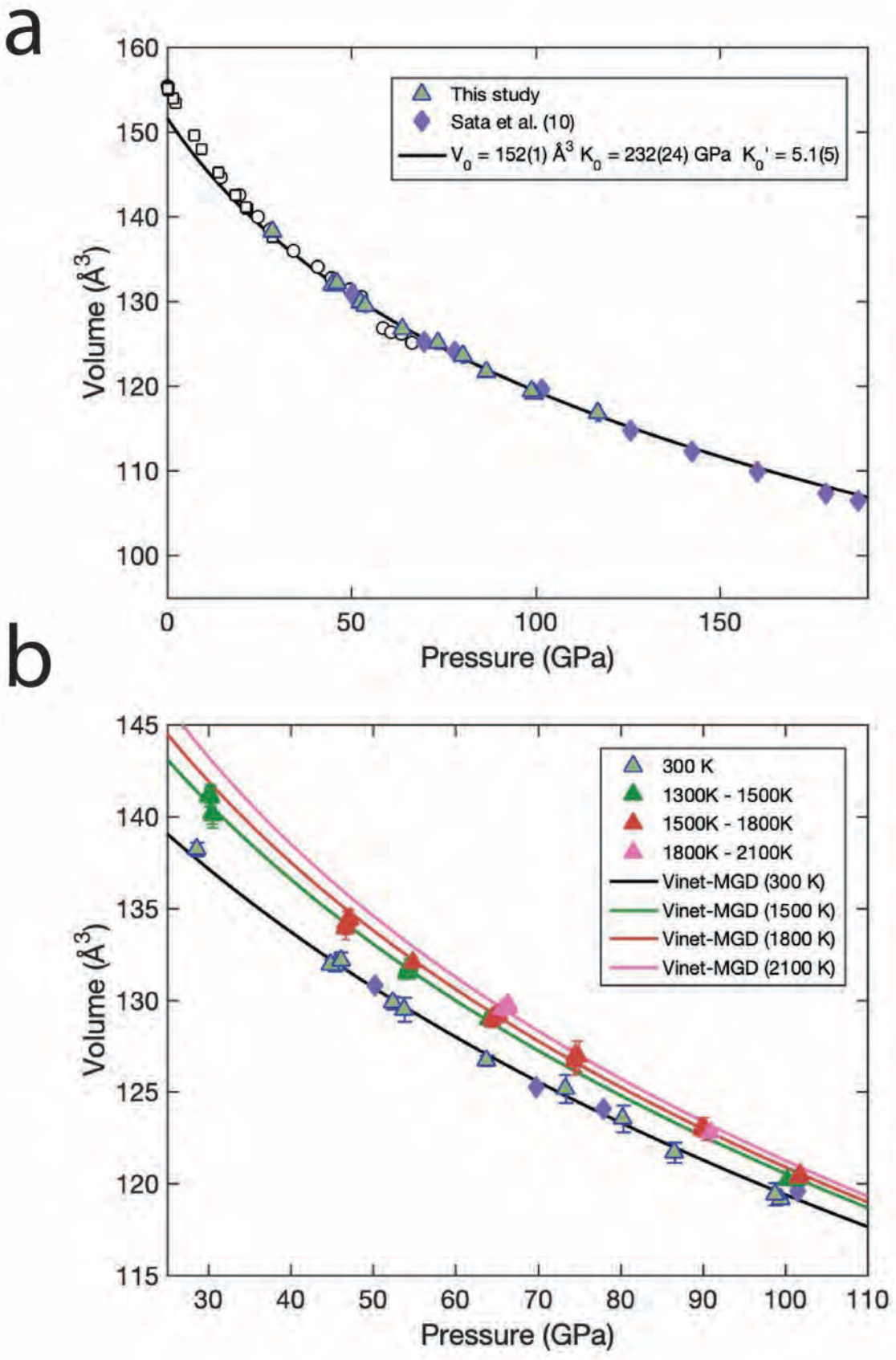
a
This study
Sata et al. (10)
V0 = 152(1) Å3 K0 = 232(24) GPa K0' = 5.1(5)
Volume (Å3)
Pressure (GPa)
b
300 K
1300K - 1500K
1500K - 1800K
1800K - 2100K
Vinet-MGD (300 K)
Vinet-MGD (1500 K)
Vinet-MGD (1800 K)
Vinet-MGD (2100 K)
Volume (Å3)
Pressure (GPa)

Figure 3

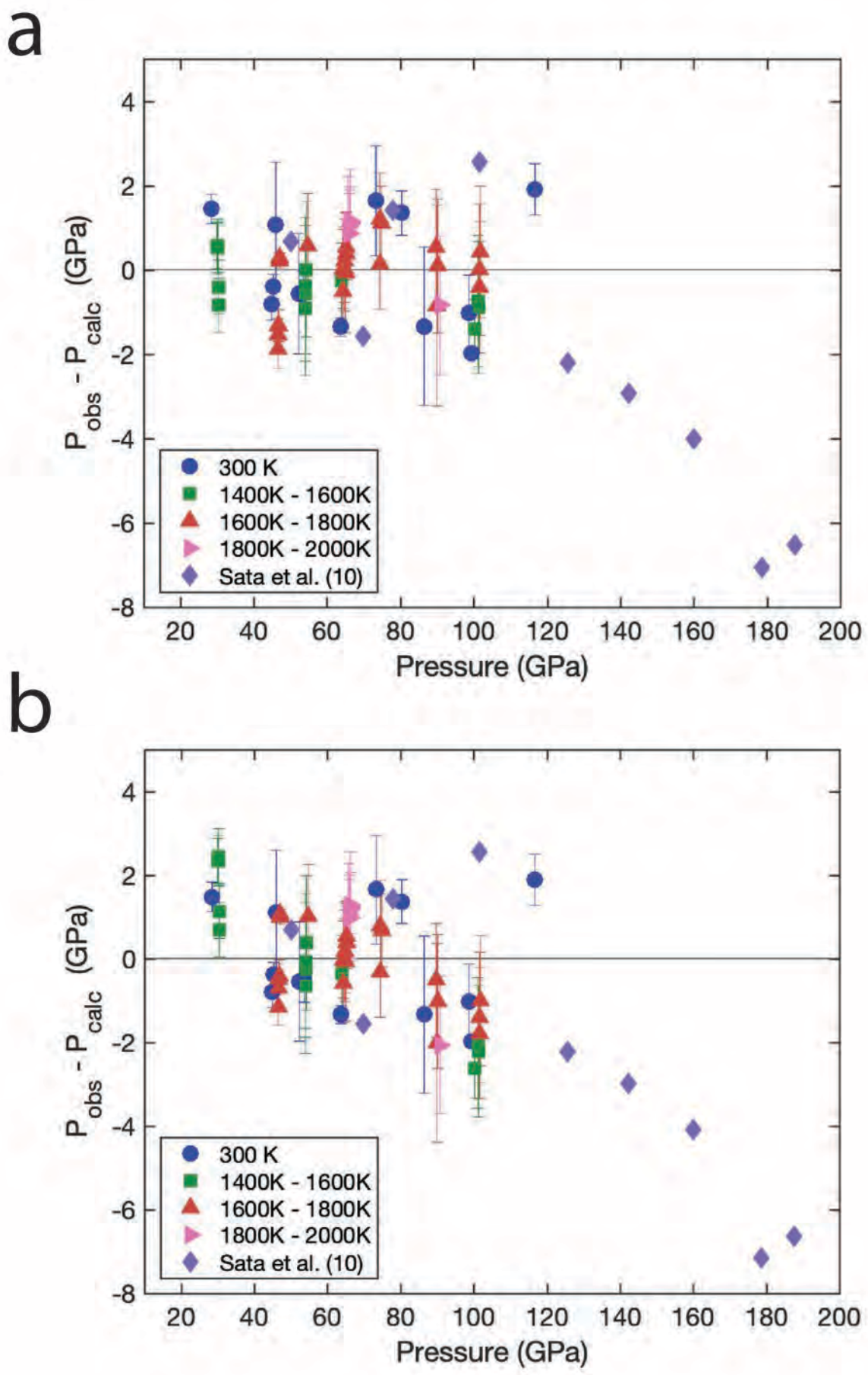
a
b
$P_{obs}$ - $P_{calc}$ (GPa)
Pressure (GPa)
300 K
1400K - 1600K
1600K - 1800K
1800K - 2000K
Sata et al. (10)
4
2
0
-2
-4
-6
-8
20
40
60
80
100
120
140
160
180
200

Figure 4

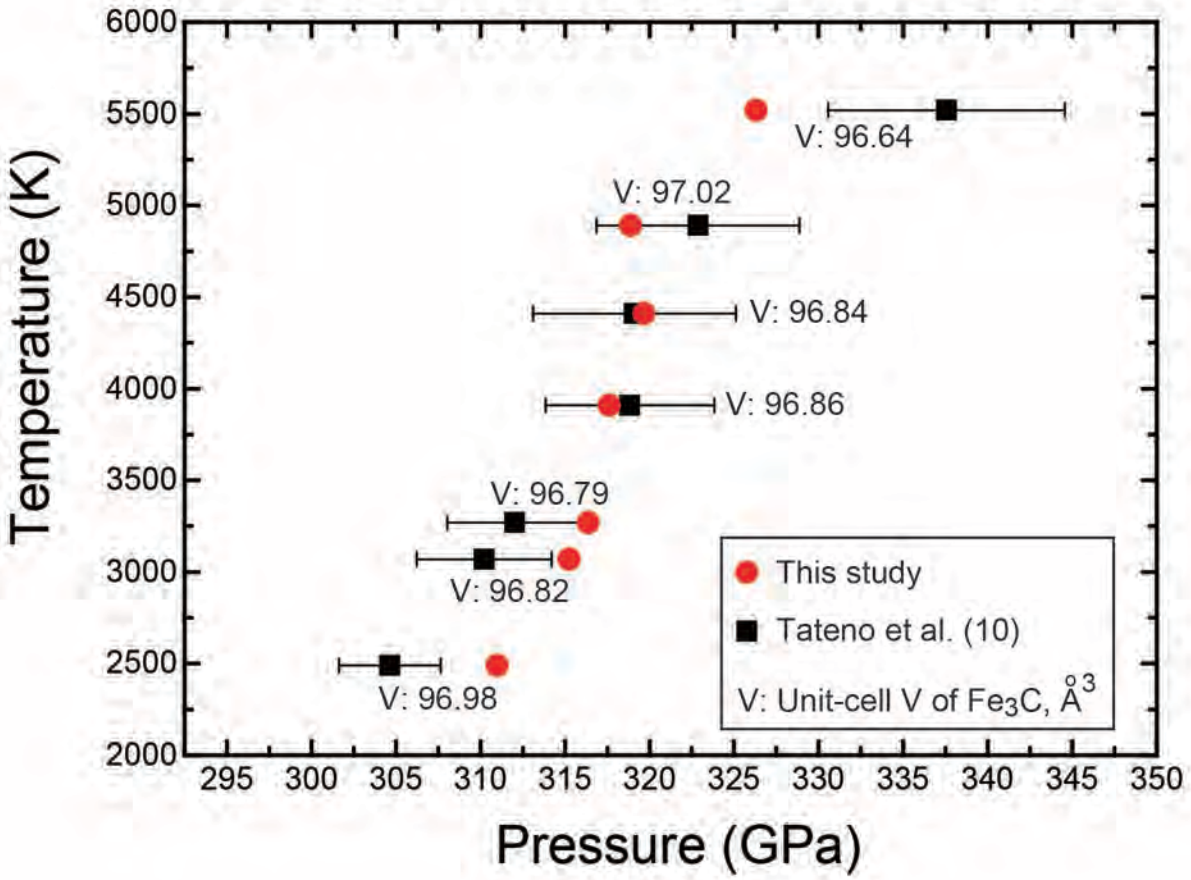
Temperature (K)
Pressure (GPa)
6000
5500
5000
4500
4000
3500
3000
2500
2000
295
300
305
310
315
320
325
330
335
340
345
350
V: 96.64
V: 97.02
V: 96.84
V: 96.86
V: 96.79
V: 96.82
V: 96.98
This study
Tateno et al. (10)
V: Unit-cell V of Fe3C, Å3

Figure 5

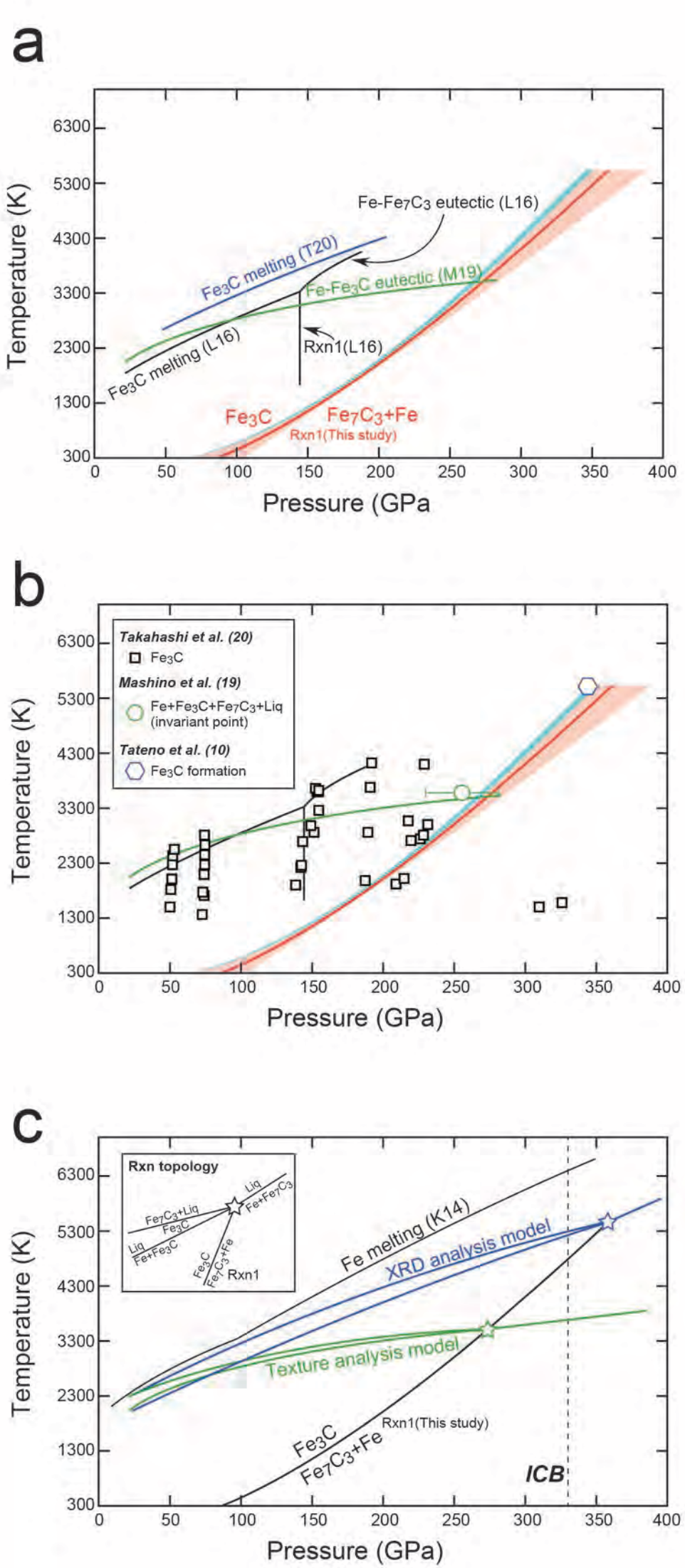
a
Temperature (K)
Pressure (GPa
Fe-Fe7C3 eutectic (L16)
Fe3C melting (T20)
Fe-Fe3C eutectic (M19)
Fe3C melting (L16)
Rxn1(L16)
Fe3C
Fe7C3+Fe
Rxn1(This study)
b
Takahashi et al. (20)
Fe3C
Mashino et al. (19)
Fe+Fe3C+Fe7C3+Liq
(invariant point)
Tateno et al. (10)
Fe3C formation
Temperature (K)
Pressure (GPa)
c
Rxn topology
Fe7C3+Liq
Fe3C
Liq
Fe+Fe3C
Liq
Fe+Fe7C3
Fe3C
Fe7C3+Fe
Rxn1
Fe melting (K14)
XRD analysis model
Texture analysis model
Fe3C
Fe7C3+Fe
Rxn1(This study)
ICB
Temperature (K)
Pressure (GPa)

Figure 6

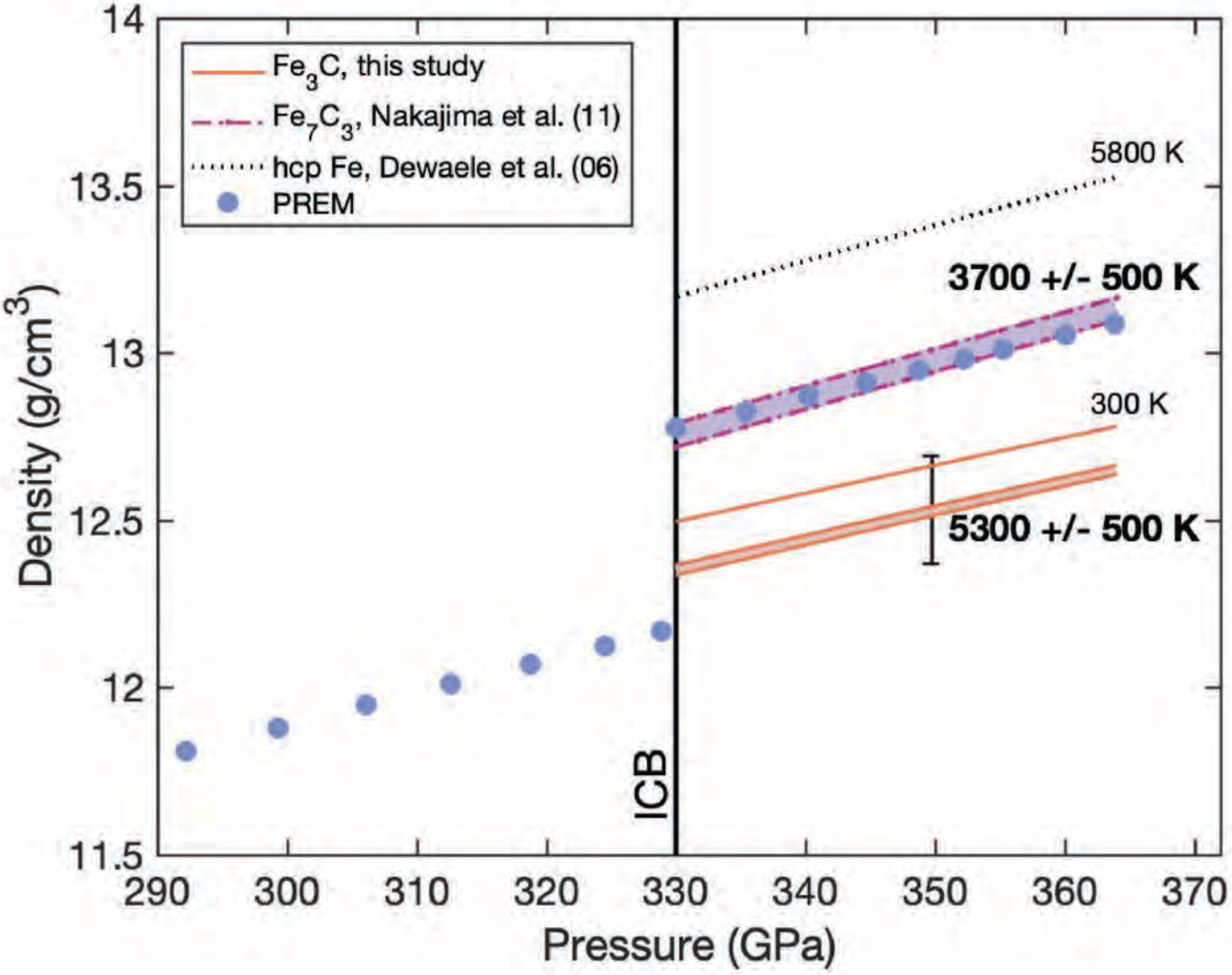
Fe3C, this study
Fe7C3, Nakajima et al. (11)
hcp Fe, Dewaele et al. (06)
PREM
5800 K
3700 +/- 500 K
300 K
5300 +/- 500 K
ICB
Density (g/cm3)
Pressure (GPa)
14
13.5
13
12.5
12
11.5
290
300
310
320
330
340
350
360
370

Figure 7